ZnON MIS Thin-Film Diodes

MOHAMAD HAZWAN MOHD DAUT [1] **(Student Member, IEEE), JOHN F. WAGER** [2] **(Fellow, IEEE), AND AROKIA NATHAN** [1,3] **(Fellow, IEEE)**

1 Department of Engineering, University of Cambridge, Cambridge CB3 0FA, U.K.
2 Department of Electrical and Computer Engineering, Oregon State University, Corvallis, OR 97331, USA
3 Cambridge Touch Technologies, Cambridge CB4 0GN, U.K.

CORRESPONDING AUTHOR: M. H. MOHD DAUT (e-mail: mhbm2@cam.ac.uk)

ABSTRACT Zinc oxynitride metal–insulator–semiconductor diodes are fabricated and characterized. Although these devices display excellent rectification, their temperature-dependent current–voltage characteristics are not explicable using analysis methodologies currently available in the literature. Therefore, we employ a simple curve fitting strategy in order to elucidate measured trends. It is found that the forward current trends are describable using three parameters, i.e., reverse saturation current, ideality factor, and series resistance, whereas the reverse current temperature dependence only requires one parameter, i.e., shunt resistance. All four of these model parameters are found to be strongly temperature dependent.

INDEX TERMS Metal oxide semiconductor, zinc oxynitride, MIS diode, thin film device.

I. INTRODUCTION

Active metal oxide semiconductor materials have been a focus in recent years due to their superior performance. Amongst other advantages, low cost, the possibility of low temperature deposition, and robust integration with other organic and inorganic compounds are key attributes. In this paper, we report on the characterization of diodes fabricated from an oxide semiconductor, with the ultimate objective of exploring the possibility of using such diodes in energy harvesting applications. One of the most extensively studied semiconductors in this group is zinc oxide (ZnO). Several ZnO diode studies have been reported [1]–[3]. In order to improve the performance of ZnO, cation and anion control strategies have been investigated and implemented. These include the formation of InGaZnO and InZnO for metal cation control and ZnON for anion control. ZnON is an attractive semiconductor material since it possesses a high mobility ($\approx$ 100 cm^2/ Vs), high illumination stability, and the ability to be deposited at room temperature [4]–[6].

Moreover, it has been shown that depending on the degree of nitrogen replacement of oxygen, the properties of ZnON can vary between ZnO and Zn_2N_3 [4]. However, since ZnON is a semiconductor with a mixture of ZnO, ZnO_xN_y, and Zn_3N_2, and since Zn possesses a higher reactivity with oxygen compared to nitrogen, ZnON has been associated with problems of stability and reproducibility, especially when exposed to air. To counter this problem, several solutions have been proposed, including argon plasma treatment [7] and heat treatment [8], [9]. In this work, we investigate the implementation of zinc oxynitride (ZnON) in a metal-insulator-semiconductor (MIS) thin-film diode structure.

The main purpose of depositing a very thin insulating layer between the metal and semiconductor is to minimize reaction and diffusion between metal and semiconductor [10]. Furthermore, the thin insulating film has been demonstrated to reduce leakage current and defect trapped charge density [11], [12], thereby improving the reliability and performance of the diode. Another advantage is the possibility of reducing the interface state density [13], [14]. In this contribution, aluminium oxide (Al_2O_3) is used as the insulating layer since the film quality and the thickness can be precisely controlled via atomic layer deposition (ALD).

ZnON MIS diode current-voltage (I-V) characteristics are modelled using [15]

$$I = I_O \left[exp\left(\frac{q(V - IR_s)}{nk_BT} \right) - 1 \right] - \frac{V - IR_s}{R_{sh}} \quad (1)$$

where I_0 is reverse saturation current, q is electronic charge, R_s is series resistance, n is ideality factor, k_B is Boltzmann's constant, T is temperature, and R_{sh} is shunt resistance. Since

the exponential term dominates when V is positive, the forward current is describable using three model parameters, i.e., I_0, n, and R_s. Conversely, since I_0 and IR_s are found to be negligibly small at negative voltage for the ZnON MIS diodes tested, the reverse current is determined by only a single model parameter, i.e., R_{sh}. In order to accurately fit experimental temperature-dependent I-V curves using eq. (1), all four model parameters are assumed to depend on temperature.

Although many parameter estimation strategies have been proposed in the literature for the direct extraction of I_0, n, R_s, and R_{sh} [16]–[22], we have been unsuccessful when employing these methods to the assessment of our ZnON MIS diodes. In contrast, we can readily estimate I_0, n, R_s using the exponential portion of eq. (1) to accurately fit to an experimental I-V curve. Moreover, we find our estimates of these parameters to be almost unique since the low, intermediate, and high current portions of the forward current are primarily determined by I_0, n, and R_s, respectively as shown in Fig. 1. From this, a fitting procedure is proposed as follows. First I_0 is estimated as the y-intercept of the low voltage portion of the curve. Next using this estimated value of I_0, n is varied whilst maintaining R_s as 0 Ω until a good fit of the low voltage portion of the curve is obtained (this region is found to be approximately linear when plotted on a semilog scale). Next, R_s is increased until a good fit to the higher voltage portion of the curve is obtained. Finally, all 3 parameters are tweaked to produce an optimal fit. This fitting is accomplished using Mathematica.

II. FABRICATION AND EXPERIMENTAL SETUP

The structure of the fabricated diode is shown in Fig. 2. The 1 mm thick Corning substrate was cleaned by first rinsing it with deionized (DI) water and then ultrasonicating it in acetone and then isopropyl alcohol solution, each for 10 minutes. It was then blow dried with nitrogen gas and subsequently baked at 120 °C for 30 minutes to remove possible moisture. Molybdenum bottom contact (100 nm) was then sputtered at room temperature. The ZnON layer (50 nm) was deposited through the reactive magnetron sputtering method by using zinc target (99.99 % purity) together with argon, nitrogen, and oxygen gases (Ar/N_2/O_2 = 4/180/1.5 SCCM) that flowed into the chamber at room temperature. The chamber pressure and RF power were maintained at 12.5 mTorr and 250 W, respectively. From the Hall measurements, the magnitude of the Hall mobility for the as-deposited ZnON film based on this formulation is 21.5 cm^2/Vs. The Al_2O_3 layer (2.5 nm) was then deposited through the atomic layer deposition (ALD) at 250 °C. Finally, a nickel top contact (100 nm) was sputtered at room temperature. The sample was then annealed at 250 °C in normal atmospheric condition for 2 hours. The annealing condition was optimised based on the improvements/degradations observed in the forward I-V characteristics after each annealing process. Shadow mask was used to pattern the semiconductor, insulator,
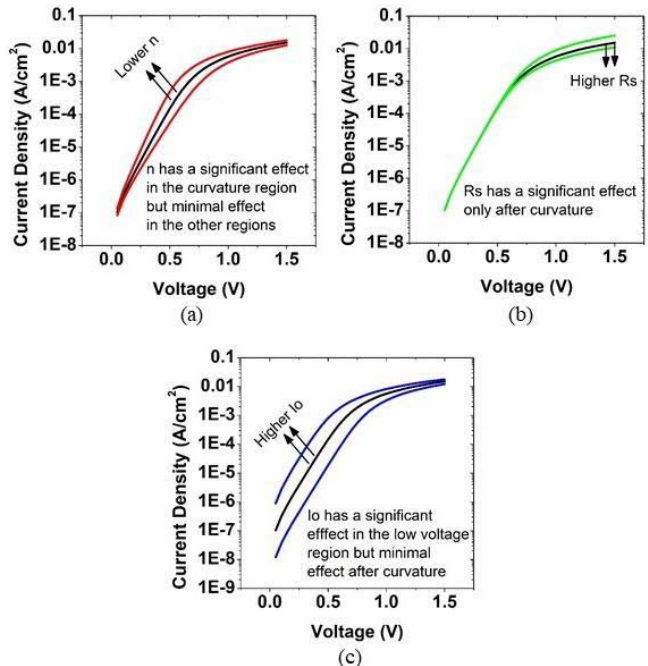

FIGURE 1. The effects of all three parameters on the J-V curve. Black lines depict the actual behavior and the red, green, and yellow lines show the effects of varying the (a) ideality factor n, (b) series resistance Rs, and (c) saturation current Io, respectively whilst maintaining identical values for the other model parameters.

and top contact layer. The active area of the diode is 0.66 mm^2.

I-V and C-V measurements were carried out using Keithley 4200 Semiconductor Characterization System (4200-SCS) inside a LakeShore probe station and the temperature was controlled using Lakeshore 336 Temperature Controller. All measurements were carried out in the dark and the temperature was varied from 50 °C to 200 °C in 50 °C intervals (323 K to 473 K in 50 K intervals). All I-V measurements were done under a vacuum environment except for room temperature measurement (normal atmosphere). The voltage for the I-V characterization for the room temperature measurements and temperature dependent measurements was swept from −3 V to +3 V with 0.2 V intervals and from −1.5 V to 1.5 V with 0.05 V intervals, respectively. The C-V sweep was carried out at 1 MHz with an ac modulation voltage of 30 mV.

III. RESULTS AND DISCUSSION
A. ROOM TEMPERATURE I-V AND C-V MEASUREMENTS
A J-V plot for a ZnON MIS diode at room temperature is shown in Fig. 3. The diode shows typical rectifying behaviour (exponential increase of current in forward bias and weak dependence in reverse bias) with a threshold voltage of approximately 0.95 V and a leakage current density of 0.4 µA/cm^2 at −3 V. Introduction of a thin interfacial layer between metal and semiconductor reduces the leakage current and likely increases the threshold voltage [12]. The
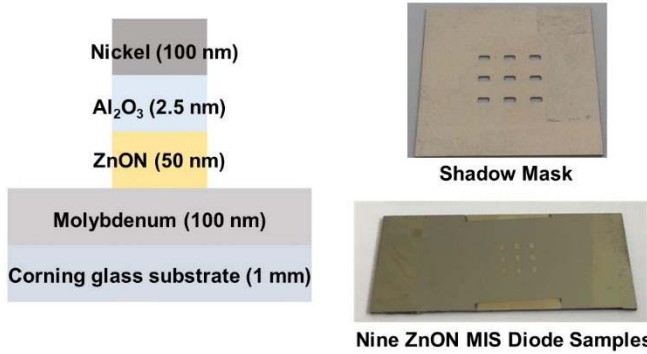
FIGURE 2. MIS diode structure and actual sample of the fabricated diode. All layers are sputter deposited except for the Al₂O₃ which is by atomic layer deposition.

TABLE 1. Parameters extracted from room temperature measurements.

Parameter	Magnitude
Ideality factor, n	2.55
Series resistance, R_s	3800 Ω
Barrier height from I-V, Φ_B	0.83 eV
Barrier height from C-V, Φ_B	0.86 eV
Shunt resistance, R_{sh}	1.3 GΩ

rectification ratio of the diode is 9500 at ± 3 V. The forward and reverse breakdown voltage of the diode are 28 and −25 V, respectively. Generally, the diode possesses a strong rectifying property.

The forward current 3-parameter curve fitting method is implemented to obtain n = 2.55, I_0 = of 1.6×10^{-10} A, and R_s = 3800 Ω. The reverse current 1-parameter fitting yields R_{sh} = 1.3 GΩ.

The n = 2.55 ideality factor is much larger than that expected for thermionic emission (n = 1) or generation-recombination (n = 2). This large value of n can be elucidated using induced gap state (IGS) theory [14], as follows. Modeling the ZnON MIS diode in non-equilibrium as a voltage divider consisting of an insulator capacitance density, C_I, in series with a parallel combination of the semiconductor and interface state capacitance densities leads to

$$n \approx 1 + \frac{C_{FB} + C_{SSmin}}{C_I} = 1 + \frac{3.6\ Fcm^2 + 1.7\ Fcm^2}{3.2\ Fcm^2} = 2.67 \quad (2)$$

where C_{FB} and C_{SSmin} are flatband and minimum interface state capacitance densities, which apply when the semiconductor is operating in depletion. This calculated value of n = 2.67 is in reasonable agreement with the measured value of n = 2.55. According to IGS theory, current in the ZnON MIS diode is thermionic, but n is large since much of the applied voltage drops across the insulator instead of the semiconductor.

The free electron carrier concentration is determined from the slope of the 1/C²-V plot as shown in Fig. 3 and inset (a). The barrier height is calculated from the built-in potential estimated by extrapolating the 1/C²-V plot [23]. From this,
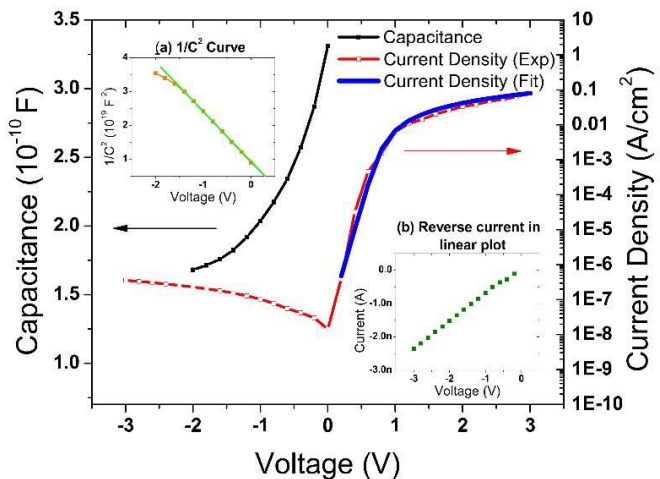
**FIGURE 3.** J-V and C-V curves for a ZnON MIS diode at room temperature. Inset (a) shows the 1/C²-V curve that is plotted in order to estimate the barrier height. Inset (b) shows an I-V plot in reverse bias, which is almost linear and is used to estimate the shunt resistance of the diode.

the calculated free electron carrier concentration and barrier height are 2.2×10^{18} cm⁻³ and 0.86 eV, respectively. An alternative way to estimate the barrier height, Φ_B, is from I-V data using [23]

$$I_O = AA^{**}T^2 exp\left(-\frac{q\Phi_b}{k_BT}\right) \quad (3)$$

where A is diode area and A** is the effective Richardson constant [24]

$$A^{**} = \frac{4\pi q m^* k^2}{h^3} \quad (4)$$

where m* is effective mass and h is Planck's constant. Assuming m* = 0.19 m_0 for ZnON [6], [25] and using $I_0 = 1.6 \times 10^{-10}$ A leads to Φ_B = 0.83 eV. Thus, our C-V and I-V estimates for Φ_B are quite similar. Parameters extracted from room temperature I-V and C-V measurements are summarized in Table 1. Table 4 presented at the end of this contribution provides overall comparison of the parameters extracted at room temperature for the diode fabricated in this contribution and other reported metal oxide diodes work.

B. TEMPERATURE DEPENDENT I-V MEASUREMENTS

Fig. 4 shows J-V curves in forward bias for a ZnON MIS diode at four temperatures. J-V characteristics depend strongly on temperature, increasing with increasing temperature. The 3-parameter fit to the measured J-V curves is quite good. Extracted fitting parameters for all curves are collected in Table 2. From Table 2, it can be observed that all four model parameters vary strongly with temperature.

Next, the reverse bias I-V curves as the function of temperature for a ZnON MIS diode are shown in Fig. 5. Using eq. (1), a linear fit of the data is used to estimate the shunt resistance. These values of R_{sh} are compiled in Table 3.
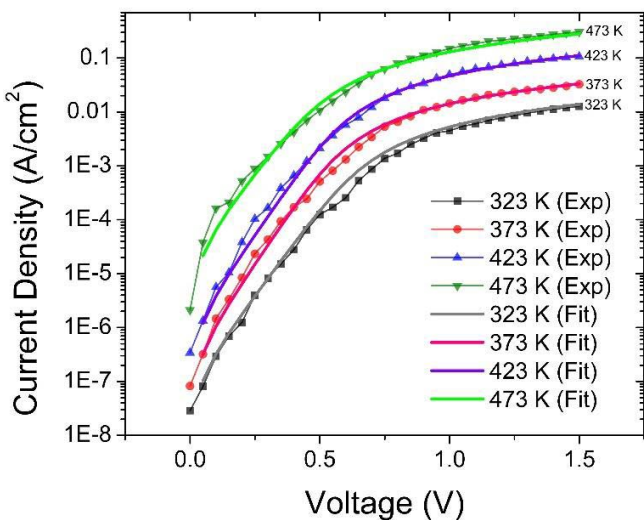
FIGURE 4. Measured (indicated as points) and fits (smooth curves) of the forward J-V curves for a ZnON MIS diode at multiple temperatures.

TABLE 2. Model parameters used to fit measured temperature-dependent I-V curves for a ZnON MIS diode.

| Temp. (K)	I_0 (A)	n	R_S (Ω)	Φ_B (eV)
323	6.15×10^{-10}	2.43	7700	0.86
373	1.68×10^{-9}	1.90	3550	0.97
423	1.12×10^{-8}	1.72	1050	1.04
473	6.56×10^{-8}	1.65	420	1.10
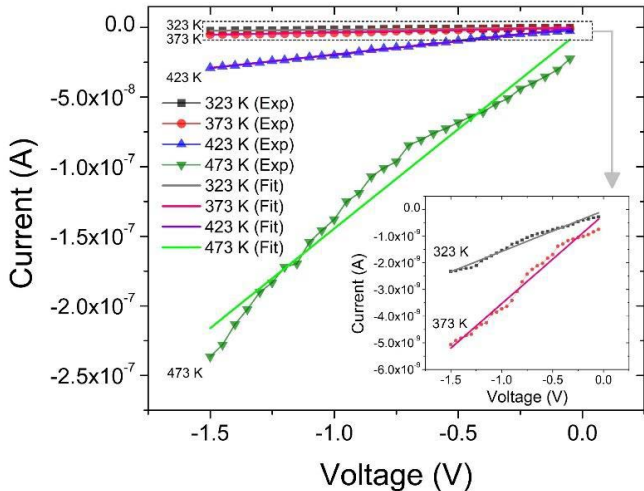
FIGURE 5. Measured (indicated as points) and fits (smooth curves) of the reverse biased curves for a ZnON MIS diode at multiple temperatures.

TABLE 3. Shunt resistance, R_{sh} as a function of temperature as estimated from measured reverse bias I-V curves for a ZnON MIS diode.

Temp. (K)	R_{sh} (GΩ)
323	0.50
373	0.33
423	0.05
473	0.01
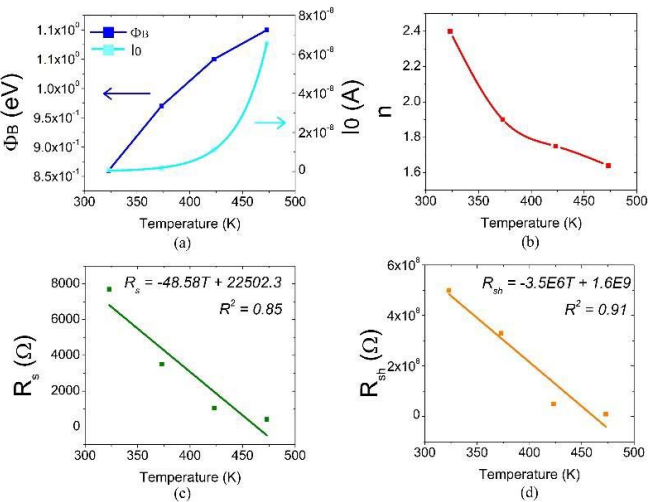
FIGURE 6. Temperature trends for model parameters used to obtain J-V fits to measured data for a ZnON MIS diode. (a) I_0 and Φ_B, (b) n, (c) R_S, and (d) R_{sh}.
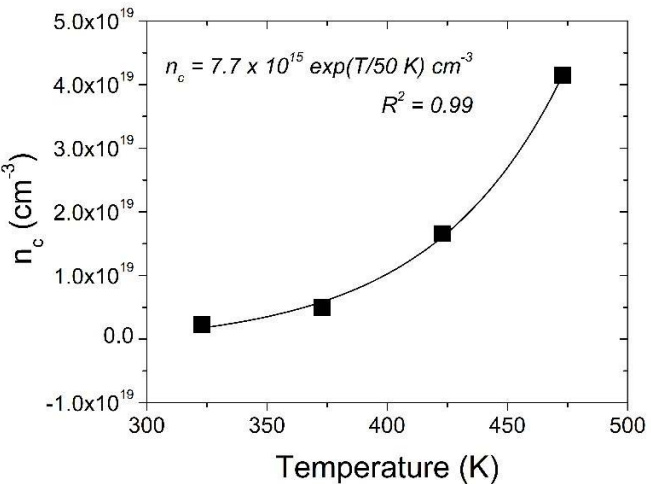
FIGURE 7. Temperature-dependent free electron carrier concentration estimated from the temperature-dependent R_S data.

All of the five extracted parameters; saturation current I_0, barrier height Φ_B, ideality factor n, series resistance R_s, and shunt resistance R_{sh} are strongly temperature dependent; temperature trends for each of these parameters are plotted in Fig. 6. I_0 increases with increasing temperature, as does Φ_B since they trend together according to eq. (3). n decreases with increasing temperature, suggesting that thermionic emission contributes more to the forward current at higher temperatures. Both R_s and R_{sh} decrease with

increasing temperature. This is ascribed to an increase in the free electron carrier concentration with increasing temperature. R_{sh} is suspected to arise from the existence of a peripheral leakage path at the edges of the diode. Thus, the decrease of R_{sh} with increasing temperature is also ascribed to an increase in the electron free carrier concentration with increasing temperature.

TABLE 4. Comparison of the extracted parameters at room temperature between the diode fabricated in this contribution and other recent reported diode work based on metal oxide semiconductors.

Ref.	Diode structure & material	Thickness (nm)	Ideality factor	Barrier height (eV)	Threshold voltage (V)	Carrier concentration (cm^{-3})	Series resistance (Ω)	Rectification ratio	Breakdown voltage (V)
[26] 2019	TiN/a-IGZO/Cu (MS)	110	1.3	0.76	0.6	5.7×10^{17}	-	3×10^6 at ± 1 V	-
[27] 2018	p-Si/n-ZnO:Al (pn)	-	1.96	0.70	-	0.9×10^{11}	6340	-	-
[28] 2018	Pd/IGZO/Ti/Au (MS)	180	1.09	0.80	-	-	-	1.3×10^6 at ± 1 V	-7.5
[29] 2018	Au/SnO$_2$/p-Si (MS)	53.5 (Au and SnO$_2$ only)	1.11 – 1.40	0.33 – 0.63	-	1×10^{20}	-	-	-
[30] 2018	Au/AZO (MS)	150 (AZO only)	10	0.39	-	-	110	-	-
[31] 2017	Pt/IGZO/Al (MS)	100 (Pt and IGZO only)	1.36	0.92	0.6	4.05×10^{18}	507	2.4×10^6 at ± 1 V	-
[32] 2017	Pd/IGZO (MS)	230	1.09	0.88	0.5	9.9×10^{13}	-	7.2×10^7 at ± 1 V	-
[33] 2017	PEDOT-PSS/a-IGZO (MS)	175	1.57	0.77	0.4	-	828	1.8×10^5 at ± 1 V	-
[34] 2017	n-IZO/p-CuO (pn)	165	10	1.16	1.4	-	-	10^4 at ± 2 V	-
[35] 2017	Pd/MgZnO/Al (MS)	-	1.87	0.62	1.9	-	-	59.9 at ± 5 V	-
[36] 2017	Pd/IGZO/Ti (MS)	230	1.15	0.73	-	2×10^{14}	33	6.8×10^4 at ± 1 V	-6
[37] 2016	Al/n-ZnO/p-Si (pn)	110 (Al and ZnO)	2.36	0.41	-	-	-	-	-
[38] 2016	Pd/IGZO/Ti (MS)	230	1.14	0.73	-	-	15	1.3×10^5 at ± 1 V	-6
[39] 2016	Pd/Zn-Sn-O/Mo (MS)	-	1.94	0.47	-	1.13×10^{17}	20	10^2 at ± 1 V	-
[40] 2016	Al/ZnO/Au (MS)	10 (ZnO only)	1.9	0.79	-	1.4×10^{18}	28000	10^6 at ± 2.5 V	-
[41] 2016	p-NiO/β-Ga$_2$O$_3$ (pn)	-	2	-	1.4	-	95	10^8 at ± 3 V	-46
[42] 2016	Pd/IGZO/Ti/Au (MS)	196	1.23	1.02	-	1.5×10^{13}	284	8.5×10^7 at ± 2 V	-
[43] 2014	Pd/IGZO/Mo (MS)	230	1.2	0.83	-	-	250	10^{10} at ± 2 V	-
[44] 2014	ITO/n-IGZO/p-Cu$_2$O/Pt (pn)	340 (IGZO and Cu$_2$O)	1.4	-	0.4	-	-	3.4×10^4 at ± 1.2 V	-
[45] 2013	Au/Ni/ZnO/ITO (MS)	1300	1.2	0.90	-	1.5×10^{15}	-	3.3×10^7 at ± 2 V	-
[46] 2012	Ag/MgZnO/ZnO/MgZnO/Ti/Au (MS)	280	2.37	0.73	0.7	-	1371	10^3 at ± 1 V	-
[47] 2010	Al/ZnO/p-Si/In (pn)	70 (ZnO)	2.7	-	1.5	-	-	3.3×10^3 at ± 3 V	-
[48] 2010	Au/Ni/ZnO/ZnO-ITO/Al (MS)	2500	1.23	0.82	1.4	-	-	1.8×10^4 at ± 2 V	-
This work	Ni/Al$_2$O$_3$/ZnON/Mo (MIS)	252.5	2.55	0.83	0.9	2.2×10^{18}	3800	9.5×10^3 at ± 3 V	-19

Evidence that the physical mechanism responsible for the temperature dependence of R_s and R_{sh} is identical is provided by the observation that their fractional decrease in resistance with increasing temperature are quite similar, i.e., R_s (T) / R_s (323 K) = 1, 0.46, 0.14, and 0.05; R_{sh} (T) / R_{sh} (323 K) = 1, 0.66, 0.1, and 0.02 for T = 323, 373, 423, and 473 K. The free electron carrier concentration is estimated for each temperature by assuming a linear relation of R_s with temperature and using the free electron carrier concentration at room temperature as obtained from C-V measurements in the previous section

$$R_s(T) = \frac{\rho(T)L}{A} \approx \frac{L}{q\mu_n n_c(T)A} \propto \frac{1}{n_c(T)} \quad (5)$$

where ρ is resistivity, L is length, μ_n is electron mobility, and n_c is free electron carrier concentration. By assuming that other parameters apart from R_s and n_c are independent of temperature, the estimated temperature-dependent free electron carrier concentration obtained is shown in Fig. 7. The regression fit to the data reveals a characteristic temperature of 50 K, corresponding to a free electron carrier concentration enhancement energy of 4 meV.

IV. CONCLUSION

In this contribution, ZnON MIS diodes are fabricated and characterized. These devices are found to exhibit excellent rectification. A fitting method is employed to describe the strongly temperature dependent forward and reverse

current characteristics of the diode. Measured forward current characteristics are accurately fit using three model parameters, i.e., saturation current, ideality factor, and series resistance while measured reverse current characteristics are fit using only one parameter, i.e., the shunt resistance.

REFERENCES

[1] H. Sheng, S. Muthukumar, N. W. Emanetoglu, and Y. Lu, "Schottky diode with Ag on (1120) epitaxial ZnO film," *Appl. Phys. Lett.*, vol. 80, no. 12, pp. 2132–2134, 2002.

[2] S. Y. Lee, E. S. Shim, H. S. Kang, S. S. Pang, and J. S. Kang, "Fabrication of ZnO thin film diode using laser annealing," *Thin Solid Films*, vol. 473, no. 1, pp. 31–34, 2005.

[3] B. N. Pal *et al.*, "Pentacene-zinc oxide vertical diode with compatible grains and 15-MHz rectification," *Adv. Mater.*, vol. 20, no. 5, pp. 1023–1028, 2008.

[4] E. Lee *et al.*, "Nanocrystalline ZnON; high mobility and low band gap semiconductor material for high performance switch transistor and image sensor application," *Sci. Rep.*, vol. 4, p. 4948, Nov. 2014.

[5] H.-S. Kim *et al.*, "Anion control as a strategy to achieve high-mobility and high-stability oxide thin-film transistors," *Sci. Rep.*, vol. 3, p. 1459, Mar. 2013.

[6] M. Ryu *et al.*, "High mobility zinc oxynitride-TFT with operation stability under light-illuminated bias-stress conditions for large area and high resolution display applications," in *Int. Electron Devices Meeting Tech. Dig. (IEDM)*, vol. 717. San Francisco, CA, USA, 2012, pp. 112–114.

[7] E. Lee *et al.*, "Ar plasma treated ZnON transistor for future thin film electronics," *Appl. Phys. Lett.*, vol. 107, no. 12, 2015, Art. no. 122105.

[8] J. Park *et al.*, "The effects of active layer thickness and annealing conditions on the electrical performance of ZnON thin-film transistors," *J. Alloys Compd.*, vol. 688, pp. 666–671, Dec. 2016.

[9] H. Jeong, H.-S. Jeong, D.-H. Kim, C.-Y. Jeong, and H.-I. Kwon, "Effects of post-deposition thermal annealing temperature on electrical properties of ZnON thin-film transistors," *IEEE Electron Device Lett.*, vol. 37, no. 6, pp. 747–750, Jun. 2016.

[10] M. M. Bülbül, S. Zeyrek, Ş. Altındal, and H. Yüzer, "On the profile of temperature dependent series resistance in Al/Si3N4/p-Si (MIS) Schottky diodes," *Microelectron. Eng.*, vol. 83, no. 3, pp. 577–581, 2006.

[11] M. Gökçen, Ş. Altındal, M. Karaman, and U. Aydemir, "Forward and reverse bias current–voltage characteristics of Au/n-Si Schottky barrier diodes with and without SnO2 insulator layer," *Phys. B Condens. Matter*, vol. 406, no. 21, pp. 4119–4123, 2011.

[12] E. Arslan *et al.*, "Electrical characterization of MS and MIS structures on AlGaN/AlN/GaN heterostructures," *Microelectron. Rel.*, vol. 51, no. 2, pp. 370–375, 2011.

[13] J. F. Wager and J. Robertson, "Metal-induced gap states modeling of metal-Ge contacts with and without a silicon nitride ultra-thin interfacial layer," *J. Appl. Phys.*, vol. 109, no. 9, 2011, Art. no. 094501.

[14] J. F. Wager and K. Kuhn, "Device physics modeling of surfaces and interfaces from an induced gap state perspective," *Crit. Rev. Solid State Mater. Sci.*, vol. 42, no. 5, pp. 373–415, 2017.

[15] J. Nelson, "The physics of solar cells," in *The Physics of Solar Cells*. London, U.K.: Imperial College Press, 2003, p. 14.

[16] H. Norde, "A modified forward I–V plot for Schottky diodes with high series resistance," *J. Appl. Phys.*, vol. 50, no. 7, pp. 5052–5053, 1979.

[17] J.-C. Manifacier, N. Brortryb, R. Ardebili, and J.-P. Charles, "Schottky diode: Comments concerning the diode parameters determination from the forward I–V plot," *J. Appl. Phys.*, vol. 64, no. 5, pp. 2502–2504, 1988.

[18] K. Sato and Y. Yasumura, "Study of forward *I–V* plot for Schottky diodes with high series resistance," *J. Appl. Phys.*, vol. 58, no. 9, pp. 3655–3657, 1985.

[19] S. K. Cheung and N. W. Cheung, "Extraction of Schottky diode parameters from forward current-voltage characteristics," *Appl. Phys. Lett.*, vol. 49, no. 2, pp. 85–87, 1986.

[20] E. K. Evangelou, L. Papadimitriou, C. A. Dimitriades, and G. E. Giakoumakis, "Extraction of Schottky diode (and p-n junction) parameters from I–V characteristics," *Solid State Electron.*, vol. 36, no. 11, pp. 1633–1635, 1993.

[21] J. H. Werner, "Schottky barrier and pn-junction I/V plots—Small signal evaluation," *Appl. Phys. A, Solids Surf.*, vol. 47, no. 3, pp. 291–300, 1988.

[22] W. Jung and M. Guziewicz, "Schottky diode parameters extraction using Lambert W function," *Mater. Sci. Eng. B Solid State Mater. Adv. Technol.*, vol. 165, nos. 1–2, pp. 57–59, 2009.

[23] V. R. Reddy, M. S. P. Reddy, B. P. Lakshmi, and A. A. Kumar, "Electrical characterization of Au/n-GaN metal–semiconductor and Au/SiO 2/n-GaN metal–insulator–semiconductor structures," *J. Alloys Compd.*, vol. 509, no. 31, pp. 8001–8007, 2011.

[24] Z. J. Horváth, "Comment on 'analysis of I–V measurements on CrSi2-Si Schottky structures in a wide temperature range,'" *Solid State Electron.*, vol. 39, no. 1, pp. 176–178, 1996.

[25] K.-C. Ok, H.-J. Jeong, H.-M. Lee, J. Park, and J.-S. Park, "Comparative studies on the physical and electronic properties of reactively sputtered ZnO and ZnON semiconductors," *Ceram. Int.*, vol. 41, no. 10, pp. 13281–13284, 2015.

[26] Q. Wu *et al.*, "A dual-functional IGZO-based device with Schottky diode rectifying and resistance switching behaviors," *IEEE Electron Device Lett.*, vol. 40, no. 1, pp. 24–27, Jan. 2019.

[27] S. Ilican, K. Gorgun, S. Aksoy, Y. Caglar, and M. Caglar, "Fabrication of p-Si/n-ZnO:Al heterojunction diode and determination of electrical parameters," *J. Mol. Struct.*, vol. 1156, pp. 675–683, Mar. 2018.

[28] L. Du *et al.*, "High-performance flexible Schottky diodes based on sputtered InGaZnO," *IEEE Electron Device Lett.*, vol. 65, no. 10, pp. 4326–4333, Oct. 2018.

[29] B. Jang, T. Kim, S. Lee, W.-Y. Lee, and J. Jang, "Schottky nature of Au/SnO2 ultrathin film diode fabricated using Sol–Gel process," *IEEE Electron Device Lett.*, vol. 39, no. 11, pp. 1732–1735, Nov. 2018.

[30] A. Shokri and L. Dejam, "Experimental and theoretical investigations on temperature and voltage dependence of an Au/AZO thin-film Schottky diode," *Int. Nano Lett.*, vol. 7, pp. 1–8, Dec. 2018.

[31] J. Zhang, Q. Xin, A. Song, and J. Zhang, "High performance Schottky diodes based on indium-gallium-zinc-oxide," *J. Vac. Sci. Technol. Vac. Surfaces Film*, vol. 34, no. 4, pp. 1–5, 2017.

[32] L. Du *et al.*, "Effects of substrate and anode metal annealing on InGaZnO Schottky diodes," *Appl. Phys. Lett.*, vol. 110, no. 1, Jan. 2017, Art. no. 011602.

[33] C.-H. Chang, C.-J. Hsu, and C.-C. Wu, "Rectified Schottky diodes based on PEDOT: PSS/InGaZnO junctions," *Org. Electron.*, vol. 48, pp. 35–40, Sep. 2017.

[34] D. I. Choudhary, "Flexible substrate compatible solution processed P-N heterojunction diodes with indium-gallium-zinc oxide and copper oxide," *Mater. Sci. Eng. B Solid State Mater. Adv. Technol.*, vol. 218, pp. 64–73, Apr. 2017.

[35] S. Singh *et al.*, "Fabrication and characterization of hydrothermally grown MgZnO nanorod films for Schottky diode applications," *Microsyst. Technol.*, vol. 23, no. 1, pp. 39–46, 2017.

[36] Q. Xin, L. Yan, L. Yuo, and S. Aimin, "Study of breakdown voltage of indium-gallium-zinc-oxide-based Schottky diode," *Appl. Phys. Lett.*, vol. 106, no. 11, Feb. 2015, Art. no. 113506.

[37] İ. Orak, "The performances photodiode and diode of ZnO thin film by atomic layer deposition technique," *Solid State Commun.*, vol. 247, pp. 17–22, Dec. 2016.

[38] Q. Xin *et al.*, "Influence of sputtering conditions on room-temperature fabricated InGaZnO-based Schottky diodes," *Thin Solid Films*, vol. 616, pp. 569–572, Oct. 2016.

[39] Y. Son, J. Li, and R. L. Peterson, "In situ chemical modification of Schottky barrier in solution-processed zinc tin oxide diode," *ACS Appl. Mater. Interfaces*, vol. 8, no. 36, pp. 23801–23809, 2016.

[40] J. Semple, S. Rossbauer, and T. D. Anthopoulos, "Analysis of Schottky contact formation in coplanar Au/ZnO/Al nanogap radio frequency diodes processed from solution at low temperature," *ACS Appl. Mater. Interfaces*, vol. 8, no. 35, pp. 23167–23174, 2016.

[41] Y. Kokubun, S. Kubo, and S. Nakagomi, "All-oxide p–n heterojunction diodes comprising p-type NiO and n-type β-Ga2O3," *Appl. Phys. Express*, vol. 9, no. 9, pp. 1–3, 2016.

[42] L. Yan *et al.*, "High performance InGaZnO-based Schottky diodes fabricated at room temperature," *Phys. Status Solidi C*, vol. 13, nos. 7–9, pp. 618–622, 2016.

[43] A. Chasin *et al.*, "High-performance a-IGZO thin film diode as selector for cross-point memory application," *IEEE Electron Device Lett.*, vol. 35, no. 6, pp. 642–644, Jun. 2014.

[44] W.-C. Chen *et al.*, "Room-temperature-processed flexible n-InGaZnO/p-Cu$_2$O heterojunction diodes and high-frequency diode rectifiers," *J. Phys. D. Appl. Phys.*, vol. 47, no. 36, 2014, Art. no. 365101.

[45] R.-H. Chang *et al.*, "Surface modification on the sputtering-deposited ZnO layer for ZnO-based Schottky diode," *J. Nanomater.*, vol. 2013, Nov. 2013, Art. no. 560542.

[46] J. H. Lee *et al.*, "Schottky diodes prepared with Ag, Au, or Pd contacts on a MgZnO/ZnO heterostructure," *Jpn. J. Appl. Phys.*, vol. 51, Sep. 2012, Art. no. 09MF07.

[47] Y. Choi *et al.*, "High current fast switching n-ZnO/p-Si diode," *J. Phys. D. Appl. Phys.*, vol. 43, no. 34, pp. 1–4, 2010.

[48] B.-T. Lai, C.-T. Lee, J.-D. Hong, S.-L. Yao, and D.-S. Liu, "Zinc oxide-based Schottky diode prepared using radio-frequency magnetron cosputtering system," *Jpn. J. Appl. Phys.*, vol. 49, Aug. 2010, Art. no. 085501.

JOHN F. WAGER received the B.S. degree in engineering physics from Oregon State University in 1977, and the M.S. and Ph.D. degrees in electrical engineering from Colorado State University in 1978 and 1981, respectively. From 1982 to 1984, he was with Hughes Research Laboratories, where he was involved in the development of compound semiconductor devices for high-speed and optoelectronic applications. He joined the Department of Electrical and Computer Engineering, Oregon State University, in 1984, where he is currently a Professor with the School of EECS. His specialization and research focus are in the areas of solid-state materials and devices. Recent research thrusts include transparent electronics, printed electronics, and photovoltaics. He is a fellow of the Society for Information Display.

AROKIA NATHAN received the Ph.D. degree in electrical engineering from the University of Alberta. He is currently the CTO and Co-Founder of Cambridge Touch Technologies, U.K. He holds the Professorial Chair of photonic systems and displays with the Department of Engineering, Cambridge University. Following post-doctoral years at LSI Logic Corporation, USA, and ETH Zurich, Switzerland, he joined the University of Waterloo, where he held the DALSA/NSERC Industrial Research Chair in sensor technology and subsequently the Canada Research Chair in nano-scale flexible circuits. He has published over 500 papers in the field of sensor technology and CAD, and thin film transistor electronics. He has co-authored 4 books. He has over 50 patents filed/awarded and has founded/co-founded four spin-off companies. He was a recipient of the 2001 NSERC E.W.R. Steacie Fellowship. In 2006, he moved to the U.K. to take up the Sumitomo Chair of Nanotechnology with the London Centre for Nanotechnology, University College London. He was a recipient of the Royal Society Wolfson Research Merit Award from University College London. He serves on technical committees and editorial boards in various capacities. He is a Chartered Engineer, U.K., a fellow of the Institution of Engineering and Technology, U.K., and an IEEE/EDS Distinguished Lecturer.

MOHAMAD HAZWAN MOHD DAUT received the M.Eng. (First Class Hons.) degree in electrical engineering from the University of Sheffield, U.K., in 2013, and the Ph.D. degree in engineering from the University of Cambridge, U.K., in 2019. His interests are in the design and development of low power energy harvesting system, including energy harvesting mechanisms, low power converters, and power flow control for paralleling multiple low power dc–dc converters. His research also covers the fabrication and characterization of thin film devices based on oxide semiconductors for the applications of flexible power circuits for low power applications.